

# Photochemical Characteristics of Silver 4-Aminobenzenethiolate; Laser-Induced Growth of Silver Nanoaggregates Probed by Raman Spectroscopy

Yoon Mi Lee,<sup>†</sup> Kwan Kim,<sup>†,\*</sup> and Kuan Soo Shin<sup>‡,\*</sup>

Department of Chemistry, Seoul National University, Seoul 151-742, Korea, and Department of Chemistry, Soongsil University, Seoul 156-743, Korea

Received: March 29, 2008; Revised Manuscript Received: May 1, 2008

Silver 4-aminobenzenethiolate (Ag-4ABT) is one of the organic–inorganic heterostructured materials that show a well-developed progression of intense X-ray reflections associated with an infinite-sheet, two-dimensional, nonmolecular layered structure, possessing also peculiar photochemical characteristics. When visible lasers are exposed to Ag-4ABT salt, its Raman spectrum changes with time, eventually becoming the same as the surface-enhanced Raman scattering (SERS) spectrum of 4-aminobenzenethiol (4ABT) adsorbed on a roughened Ag substrate. The growth of Raman peaks of Ag-4ABT salt was monitored as a function of laser exposure time as well as laser power and wavelength. It was analyzed in terms of the symmetry types of the vibrational modes of 4ABT, and greatly enhanced  $b_2$  vibrational bands were observed in the spectra caused by the strong contribution of chemical enhancement. The signal enhancement by the exposure of the visible lasers can be attributed to the presence of SERS-active Ag nanoparticles produced by the photoreaction of Ag-4ABT salt.

## 1. Introduction

The surface-enhanced Raman scattering (SERS) is a phenomenon in which the scattering cross sections of molecules adsorbed on certain metal surfaces are dramatically enhanced.<sup>1–3</sup> In recent years, it has been reported that even single-molecule detection is possible by SERS,<sup>4–7</sup> suggesting that the enhancement factor (EF) can reach as much as  $10^{14}$ – $10^{15}$ ; the effective Raman cross sections are then comparable to the usual fluorescence cross sections. It has long been believed that two enhancement mechanisms, one called a long-range electromagnetic effect<sup>7,8</sup> and the other called a short-range chemical effect,<sup>9–11</sup> are simultaneously operative for SERS, and factors of at least 8–10 orders of magnitude can arise from electromagnetic surface plasmon excitation, while the enhancement factor due to chemical effects is of order  $10^1$ – $10^2$ . The details of the electromagnetic and chemical enhancement mechanisms have not yet been clearly unraveled, however.

It is well known that silver alkane thiolate salt (AgSR) consists of an infinite-sheet, two-dimensional (2D), nonmolecular layered structure. The alkyl chains even in  $\text{AgS}(\text{CH}_2)_4\text{CH}_3$  possess fully extended all trans conformation. Silver alkane carboxylate salt ( $\text{AgCO}_2\text{R}$ ) was also reported to consist in a layered structure.<sup>12–18</sup> These layered silver salts have unique thermal characteristics. For instance, the AgSR shows liquid crystalline behavior upon melting.<sup>16</sup> The thermal characteristics of  $\text{AgCO}_2\text{R}$  are different from those of AgSR. For the case of silver stearate (Ag-STA), for instance, two noticeable changes take place upon heating. The first phase transition takes place that can be associated with a premelting event characterized by the formation of gauche conformers at 390–420 K. A second phase transition takes place in which silver nanoparticles with a size of  $\sim 4$  nm are formed by thermal decomposition of Ag-

STA at 520–550 K. These silver nanoparticles, derivatized by stearate, readily spread as a monolayer at air/water interface, and can be packed in 3D assemblies by the Langmuir–Blodgett method.<sup>19,20</sup>

Silver aromatic thiolate salt ( $\text{AgS}\emptyset$ ) and silver aromatic carboxylate salt ( $\text{AgCO}_2\emptyset$ ) also have layered structure. Their thermal characteristics are similar to those of aliphatic salts. For instance, the binding state of the carboxylate group of silver 4-nitrobenzoate (Ag-4NBA) changes from bridging to unidentate at  $\sim 380$  K, and a second dramatic structural change occurs at  $\sim 590$  K, producing 4NBA-capped Ag nanoparticles.<sup>21</sup> The latter transition temperature for Ag-4NBA is about 80 K higher than that for Ag-STA,<sup>20</sup> and such enhanced thermal stability of Ag-4NBA is associated with the conjugation of the carboxylate group to the aromatic ring. These aromatic silver salts have also peculiar photoreaction characteristics.<sup>22,23</sup> When an argon ion laser is exposed to silver benzenethiolate salt (Ag-BT), for instance, its Raman spectrum changes with time, eventually becoming the same as the SERS spectrum of benzenethiol adsorbed on a roughened Ag substrate. Similarly, the Raman spectrum of silver 4-aminobenzoate (Ag-4ABA) becomes the same as the SERS spectrum of 4-aminobenzoic acid assembled on SERS-active Ag.<sup>24</sup> According to X-ray photoelectron spectroscopic and scanning electron microscopic studies, the SERS activity must arise due to the formation of Ag nanoaggregates caused by the irradiation of a visible laser.<sup>23</sup> As another example, the photochemical characteristics of silver 4-nitrobenzoate (Ag-4NBA) has been recently studied, and it was found that the Raman spectrum of Ag-4NBA taken using the 514.5 nm line as the excitation source eventually becomes identical to the SERS spectrum of 4-aminobenzoic acid adsorbed on Ag.<sup>21</sup> Nonetheless, the laser-induced formation of Ag nanoaggregates by the irradiation of visible lasers has not yet been clarified whether it is due to the thermolysis process or due to the photolysis process, and also the exact mechanism by which Ag nanoaggregates are formed from silver aromatic thiolate ( $\text{AgS}\emptyset$ ) or carboxylate ( $\text{AgCO}_2\emptyset$ ) salts has not yet been fully understood.

\* To whom correspondence should be addressed. (K.K.) E-mail: kwankim@snu.ac.kr. Tel: +82-2-8806651. Fax: +82-2-8891568. (K.S.S.) E-mail: kshin@ssu.ac.kr. Tel: +82-2-8200436. Fax: +82-2-8244383.

<sup>†</sup> Seoul National University.

<sup>‡</sup> Soongsil University.

4-Aminobenzenethiol (4ABT) is one of very unique adsorbate molecules whose SERS spectral patterns are known to be noticeably dependent on the relative contribution of chemical enhancement mechanism versus electromagnetic enhancement mechanism. Borne this in mind, we have investigated in this work the photoresponses of silver 4-aminobenzenethiolate salt (Ag-4ABT) by taking a series of Raman spectra as functions of laser exposure time. SERS-active Ag nanoaggregates are indeed formed by the photolysis of Ag-4ABT, showing SERS spectra of 4ABT adsorbed on Ag. The growth of SERS peaks of 4ABT has thus been analyzed in terms of the symmetry types of the vibrational modes. This information is utilized to assess which vibrational modes are more deeply associated with the chemical enhancement of 4ABT at silver nanoaggregates.

## 2. Experimental Section

Silver nitrate ( $\text{AgNO}_3$ , 99+%), 4-aminobenzenethiol (4ABT, 97%), and sodium borohydride ( $\text{NaBH}_4$ , 99%) were purchased from Aldrich and used as received. Other chemicals, unless specified, were all reagent grade, and highly pure water whose resistivity was greater than  $18.0 \text{ M}\Omega \cdot \text{cm}$  was used throughout.

To prepare silver 4-aminobenzenethiolate (Ag-4ABT), an ethanolic solution of  $\text{AgNO}_3$  (2 mmol, 20 mL) was added dropwise to an equimolar 4ABT in ethanol. The mixture was stirred vigorously during preparation; the reaction was actually carried out in an Al foil-wrapped flask to minimize light exposure. After the mixture was stirred for 1 h, a yellow precipitate of Ag-4ABT was readily produced in nearly 100% yield. The precipitate was then filtered, rinsed thoroughly with ethanol and water successively and dried under vacuum at  $150^\circ\text{C}$ . Pellets were made for Raman measurements. The silver nanoparticles were prepared by following the recipes in the literature.<sup>25</sup> Approximately, 10 mL of 1 mM  $\text{AgNO}_3$  solution was added dropwise to 30 mL of 2 mM  $\text{NaBH}_4$  solution which was cooled to ice temperature. For the self-assembly of 4-ABT on Ag sol, an ethanol solution of 4-ABT was added to the as-prepared Ag sol to give a final adsorbate concentration of  $\sim 2 \times 10^{-5} \text{ M}$ .

Raman spectra were obtained using a Renishaw Raman system Model 2000 spectrometer equipped with an integral microscope (Olympus BH2-UMA). The 514.5 nm line from a 20 mW  $\text{Ar}^+$  laser (Melles-Griot Model 351MA520) or the 632.8 nm line from a 17 mW He/Ne laser (Spectra Physics Model 127) was used as the excitation sources, and Raman scattering was detected over a  $180^\circ$  range with a Peltier cooled ( $-70^\circ\text{C}$ ) charged-coupled device (CCD) camera ( $400 \times 600$  pixels). The laser beam was focused onto a spot approximately  $2 \mu\text{m}$  in diameter with an objective microscope on the order of  $20\times$ . The holographic grating (1800 grooves/mm) and the slit allowed the spectral resolution to be  $1 \text{ cm}^{-1}$ . The Raman band of a silicon wafer at  $520 \text{ cm}^{-1}$  was used to calibrate the spectrometer, and the accuracy of the spectral measurement was estimated to be better than  $1 \text{ cm}^{-1}$ . To obtain a normal Raman spectrum of the salt pellet, the pellet was spun at 3000 rpm to minimize the laser induced photoreaction. X-ray diffraction (XRD) patterns were obtained on a Bruker D5005 powder diffractometer for a  $2\theta$  range of  $3$  to  $50^\circ$  at an angular resolution of  $0.05^\circ$  using  $\text{Cu K}\alpha$  ( $1.5406 \text{ \AA}$ ) radiation. Field emission scanning electron microscopy (FE-SEM) images were obtained with a JSM-6700F field emission scanning electron microscope operated at 5.0 kV. Transmission electron microscopy (TEM) images were acquired on a Hitachi H-7600 transmission electron microscope operated at 100 kV. Thermogravimetric analysis (TGA) and differential scanning calorimetry (DSC) data were obtained with a TA

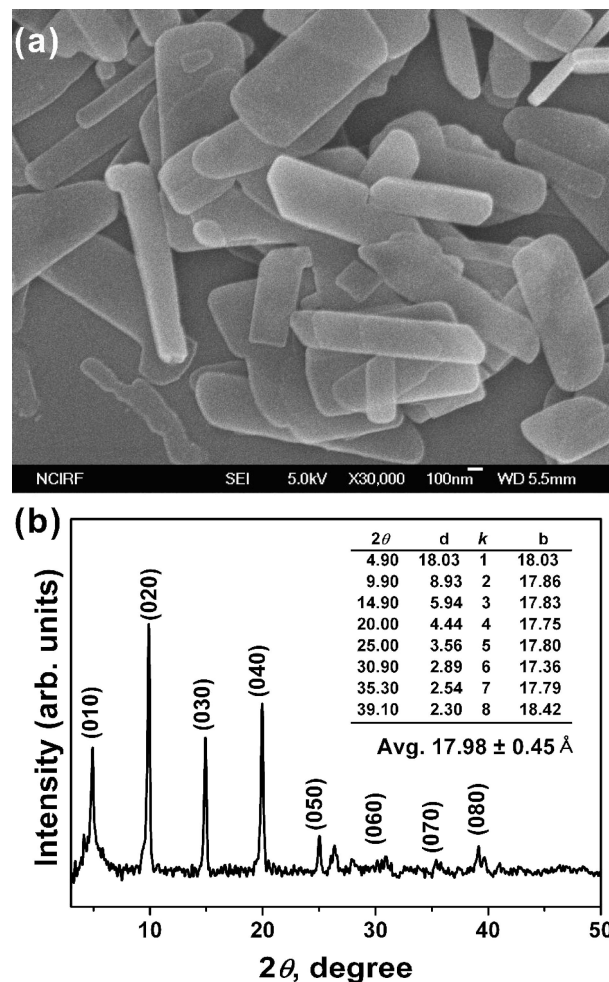


**Figure 1.** (a) FE-SEM image and (b) XRD pattern of Ag-4ABT. The interlayer spacings derived from different reflections are listed in the inset.

Instrument 2050 thermogravimetric analyzer in a nitrogen atmosphere at a heating rate of  $10^\circ\text{C}/\text{min}$ .

## 3. Results and Discussion

Figure 1a shows a typical FE-SEM image of the synthesized silver 4-aminobenzenethiolate (Ag-4ABT) salt. Micrometer-sized platelets were identified as possessing a layered structure from XRD shown in Figure 1b. The XRD pattern shows a well-developed progression of intense reflections. These intense reflections can be interpreted in terms of three dimensionally stacked silver thiolate layers with a measurable interlayer lattice dimension.<sup>12–17</sup> The layered structure of Ag-4ABT salt is schematically drawn in Figure 2. Each layer of silver thiolate is separated from the neighboring layer by twice the length of the 4-aminophenyl ring. In this sense, all intense reflections can be indexed as  $(0\ k\ 0)$  as assigned in Figure 1b. In the inset of Figure 1b, we list the interlayer spacings derived from different reflections. The averaged interlayer thickness, i.e., the sum of  $2t_1$  and  $2t_2$  in Figure 2, is then  $17.98 \pm 0.45 \text{ \AA}$ .

For better interpretation of the Raman spectra, we first needed to determine the vibrational assignment of 4-aminobenzenethiol (4ABT) in its neat state. Figure 3a,b shows the normal Raman (NR) spectra of 4-ABT in its neat solid state and anionic state in alkaline solution (pH 10), respectively, obtained using 514.5 nm radiation as the excitation source; the peak intensities as well as the peak positions were all normalized with respect to

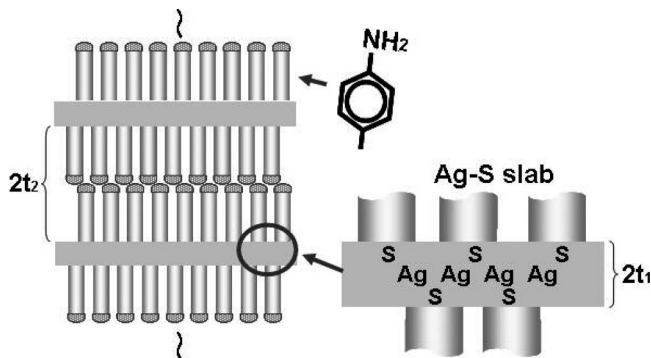


Figure 2. Schematic depiction of layered structure of Ag-4ABT salt.

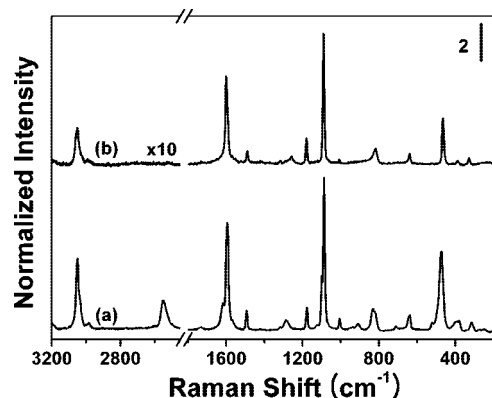


Figure 3. Normal Raman spectra of 4ABT (a) obtained from neat solid state and (b) from anionic state in alkaline solution using the 514.5 nm line of an Ar<sup>+</sup> laser as excitation source. All spectral intensities were normalized with silicon wafers.

the Raman band of a silicon wafer appearing at 520 cm<sup>-1</sup>. The NR spectra of 4ABT in its neat and anionic states were also obtained using 632.8 nm radiation from a He/Ne laser as an excitation source. The normalized Raman spectral patterns are barely dependent on the excitation wavelength. Any spectral difference between neat and anionic states is due to the deprotonation of the thiol in the anionic state. The S–H stretching band is seen at 2550 cm<sup>-1</sup> in the neat solid state spectrum but is completely missing in the alkaline solution spectrum. Major peaks in Figure 3 are collectively summarized in Table 1 along with their vibrational assignment.

We monitored the laser-induced growth of Raman peaks of Ag-4ABT as functions of laser exposure time as shown in Figure 4. When a pellet of Ag-4ABT salt was exposed to the 632.8 nm radiation from a He/Ne laser it darkened as the laser exposure time increased; the power at the sampling position was ~0.2 mW and the signal acquisition time was 10 s. Upon increasing the irradiation time, the 7a band ( $\nu$ CS) at ~1075 cm<sup>-1</sup> gradually increases and several new peaks are emerging, for instance, at 1434, 1388, and 1140 cm<sup>-1</sup>. As we will discuss later, these new peaks are all belonging to b<sub>2</sub>-type modes of 4-ABT molecule and their apparent enhancement has been ascribed in the literature to the charge-transfer (CT) from metal to the adsorbed molecule.<sup>26,27</sup> In this specific case that the power at the sampling position is ~0.2 mW of 632.8 nm radiation from a He/Ne laser, the Raman signal approaches a plateau after ~10 min. The inset of Figure 4 shows the growth of the 7a band of 4ABT at ~1075 cm<sup>-1</sup> arising from Ag-4ABT salt as a function of the laser exposure time with different laser powers of a He/Ne laser (632.8 nm). Herein, the background signal that accompanies each spectrum has been subtracted. The spectra

therefore relatively reflect the effective growth of the 7a band of 4ABT at 1075 cm<sup>-1</sup>. Increasing the laser power (and/or the signal acquisition time) causes the plateau level to be achieved in a shorter time. As can be deduced from the Figure 4, the Raman signal of Ag-4ABT is amplified up to ~20 times by the exposure to a He/Ne laser. The signal enhancement is obviously due to the presence of SERS-active Ag nanoparticles produced by the photoreaction of Ag-4ABT (*vide infra*).

To gain more insight into the wavelength dependence of the laser-induced growth of Ag nanoaggregates from Ag-4ABT salt, we have also performed Raman measurements for a pellet of Ag-4ABT using 514.5 nm from an Ar<sup>+</sup> laser. Figure 5 shows the SERS spectrum thus obtained using the 514.5 nm radiation as the excitation source, in which the laser power at the sampling position was ~0.02 mW and the signal acquisition time was 10 s. In this case, the Raman signal approaches a plateau within 10 min of laser irradiation from an Ar<sup>+</sup> laser. In the case of 632.8 nm where radiation from a He/Ne laser was used as the excitation source, it took about 10 min with the laser power at the sampling position being ~0.2 mW to reach the plateau in the growth of the Raman signal. However, when the 514.5 nm radiation was used as the excitation source, the needed laser power to approach a plateau within 10 min was only ~0.02 mW (about 10% of the laser power from a He/Ne laser). Although the laser-induced growth of Ag nanoaggregates from Ag-4ABT salt occurs quite noticeably by the irradiation of a He/Ne laser at 632.8 nm, the laser-induced growth occurs much faster using an Ar<sup>+</sup> laser at 514.5 nm. This excitation-wavelength dependence strongly suggests that the growth of Ag nanoaggregates from Ag-4ABT salt is induced from the photoreactions rather the thermolysis. All the peak positions in Figures 4 and 5 and their proper vibrational assignments are again collectively summarized in Table 1.

When a pellet of Ag-4ABT salt was illuminated by the 514.5 nm from an Ar<sup>+</sup> laser with the laser power at the sampling position being ~1 mW, it darkened quickly. Hence, it was necessary to rotate (3000 rpm) the pellet to minimize such a laser-induced change. We should mention that at least under spinning, the Raman signal is invariant, suggesting that the spectrum of Figure 6a is a NR spectrum of Ag-4ABT salt obtained using 514.5 nm radiation as the excitation source. It is seen that the NR spectral patterns of Ag-4ABT salt are quite similar to those of 4ABT in its anionic state as shown in Figure 3b. Most of the peaks in Figure 3 are correlated fairly well to each other with comparable relative intensities. The Raman spectrum of Figure 6b obtained in static condition using 514.5 nm radiation, in the signal acquisition time of 10 s with the laser power at the sampling position being ~0.2 mW, is obviously different from that of Figure 6a. As mentioned in the Introduction, the dissimilar spectral pattern in Figure 6b is due to the fact that it is indeed SERS spectrum rather than NR spectrum. The similar spectral pattern with Figure 6b was again obtained using the 632.8 nm radiation in static condition as shown in Figure 6c; the signal acquisition time was 10 s and the laser power at the sampling position was ~1 mW. It is then unsurprising that the spectral patterns of Figure 6b,c are comparable to those of Figure 6d, representing the SERS spectrum of 4ABT assembled on borohydride reduced Ag nanoparticles (4ABT@Ag). Looking more closely at the spectra in Figure 6, the most significant changes are observed in the region of 1600–1000 cm<sup>-1</sup>. Specifically, five strong peaks are observed in Figure 6b,d at 1577, 1436, 1390, 1143, and 1077 cm<sup>-1</sup>, whereas strong and medium-strong peaks are observed in Figure 6a differently at 1598, 1491, 1180, and 1087 cm<sup>-1</sup>.



**TABLE 1: Raman Spectral Peak Assignment of 4-Aminobenzenethiol (4ABT), Silver 4-Aminobenzene Thiolates (Ag-4ABT), and 4-Aminobenzenethiol Adsorbed on Colloidal Silver Particles (4ABT@Ag)<sup>a</sup>**

normal Raman			SERS			assignment <sup>b</sup>
4ABT		Ag-4ABT	Ag-4ABT		4ABT@Ag	
neat solid	anionic state	spinning	514.5 nm	632.8 nm	514.5 nm	
3051(0.46) <sup>c</sup>	3051(0.29)	3048(0.41)				$\nu$ CH, 2(a <sub>1</sub> )
3036(0.22)	3029(0.08)	3030(0.11)				$\nu$ CH, 13(a <sub>1</sub> )
2550(0.18)						$\nu$ SH
1734(0.01)	1730(0.01)					
1617(0.17)					1627(0.25)	$\delta$ NH
1594(0.70)	1599(0.64)	1598(0.62)	1590(1.19)	1588(0.82)		$\nu$ CC, 8a(a <sub>1</sub> )
1569(0.06)	1568(0.05)	1570(0.16)	1572(2.14)	1572(1.01)	1577(1.15)	$\nu$ CC, 8b(b <sub>2</sub> )
1493(0.13)	1489(0.09)	1491(0.10)		1487(0.08)		$\nu$ CC + $\delta$ CH, 19a(a <sub>1</sub> )
			1470(0.23)	1471(0.14)	1473(0.43)	
1424(0.01)	1416(0.01)		1435(1.74)	1434(0.68)	1436(3.68)	$\nu$ CC + $\delta$ CH, 19b(b <sub>2</sub> )
			1390(1.07)	1388(0.57)	1390(2.10)	$\nu$ CC + $\delta$ CH, 3(b <sub>2</sub> )
1318(0.02)	1316(0.02)			1300(0.15)	1305(0.18)	$\nu$ CC + $\delta$ CH, 14(b <sub>2</sub> )
1285(0.06)						$\nu$ CH, 7a(a <sub>1</sub> )
			1186(0.32)		1190(0.40)	
1178(0.14)	1180(0.20)	1180(0.19)		1177(0.19)		$\delta$ CH, 9a(a <sub>1</sub> )
			1140(1.38)	1140(0.80)	1143(2.20)	$\delta$ CN, 9b(b <sub>2</sub> )
1122(0.02)						
1100(0.35)						
1087(1.00)	1090(1.00)	1087(1.00)	1076(1.00)	1075(1.00)	1077(1.00)	$\nu$ CS, 7a(a <sub>1</sub> )
		1043(0.25)				
1006(0.07)	1007(0.03)		1006(0.13)	1004(0.14)	1006(0.10)	$\gamma$ CC + $\gamma$ CCC, 18a(a <sub>1</sub> )
938(0.01)						$\pi$ CH, 17a(a <sub>2</sub> )
			920(0.12)	921(0.04)	921(0.15)	$\pi$ CH, 5b(b <sub>1</sub> )
909(0.04)						$\delta$ SH
831(0.15)		826(0.06)	827(0.05)		826(0.03)	$\pi$ CH, 10a(a <sub>2</sub> )
820(0.12)	818(0.12)	814(0.13)	810(0.03)	813(0.09)		$\pi$ CH, 11(b <sub>1</sub> )
		800(0.10)				$\nu$ CH + $\nu$ CS + $\nu$ CC, 1(a <sub>1</sub> )
				750(0.02)		$\pi$ CH, 10b(b <sub>2</sub> )
711(0.02)		699(0.05)	721(0.08)	717(0.06)	719(0.10)	$\pi$ CH + $\pi$ CS + $\pi$ CC, 4b(b <sub>1</sub> )
639(0.09)	639(0.08)	634(0.12)	628(0.10)	633(0.14)	627(0.03)	$\gamma$ CCC, 12(a <sub>1</sub> )
			543(0.07)	541(0.04)	543(0.13)	
520(0.05)	524(0.01)			531(0.04)		$\gamma$ CCC, 16b(b <sub>1</sub> )
		506(0.04)				
		491(0.03)			489(0.05)	
473(0.52)	465(0.36)				463(0.03)	$\gamma$ CCC, 6a(a <sub>1</sub> )
				437(0.01)		
392(0.06)	389(0.02)	396(0.26)		404(0.19)	409(0.05)	$\tau$ CC, 16a(a <sub>2</sub> )
				390(0.21)	392(0.03)	
314(0.06)	328(0.05)					$\delta$ CH + $\delta$ CS, 18b(b <sub>2</sub> )
274(0.01)						
250(0.02)						$\delta$ CH + $\delta$ CS, 9b(b <sub>2</sub> )

<sup>a</sup> Units in wavenumber (cm<sup>-1</sup>). <sup>b</sup> Taken from refs 26 and 31:  $\nu$ , stretch;  $\delta$  and  $\gamma$ , bend;  $\pi$ , wagging; and  $\tau$ , torsion. <sup>c</sup> Normalized with respect to 7a ( $\nu$ CS) band.

Much the same observations were made by Osawa et al. in their SERS study of 4ABT on Ag island films.<sup>26</sup>

It is very intriguing that these spectral differences are deeply associated with the symmetry types of the vibrational modes. Under an assumption that 4ABT belongs to a  $C_{2v}$  point group, the benzene ring vibrations of 4ABT can be classified as a<sub>1</sub>, a<sub>2</sub>, b<sub>1</sub>, and b<sub>2</sub> species, and letting further the molecular plane be the yz plane with z aligned to the C<sub>2</sub> axis, the a<sub>1</sub> and b<sub>2</sub> species are the in-plane modes, whereas the a<sub>2</sub> and b<sub>1</sub> species are the out-of-plane modes. In principle, all these modes should be Raman active. Surprisingly, however, all the peaks observed in Figure 6b–d are due to the b<sub>2</sub> modes except the one at 1076 cm<sup>-1</sup> belonging to the a<sub>1</sub> mode. The exclusive enhancement of the b<sub>2</sub> modes may be indicative of the standing-up orientation of 4ABT on Ag in conformity with the models suggested by Creighton<sup>28</sup> and by Moskovits and Suh.<sup>29</sup> Osawa et al.<sup>26</sup> clearly revealed by potential and excitation wavelength dependence study that the exclusive appearance of the b<sub>2</sub> bands was due to the dominant contribution of the chemical enhancement mechanism specifically in the system of 4ABT on silver.

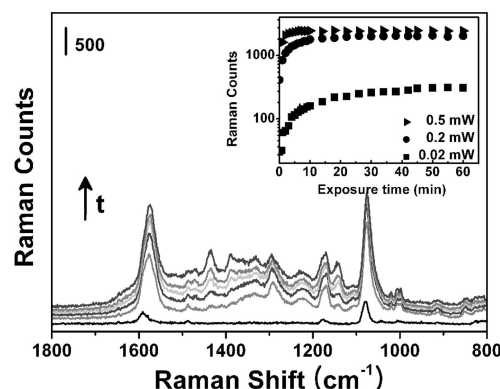


**Figure 4.** A series of Raman spectra of Ag-4ABT taken as a function of the laser exposure time using the 632.8 nm radiation as the excitation source with the laser power at the sampling position being  $\sim 0.2$  mW and the signal acquisition time being 10 s. The inset shows the growth of the 7a band of 4ABT at 1075 cm<sup>-1</sup> taken using the 632.8 nm line of a He/Ne laser as a function of the laser exposure time with laser powers of  $\sim 0.02$ ,  $\sim 0.2$ , and  $\sim 0.5$  mW at the sampling position.

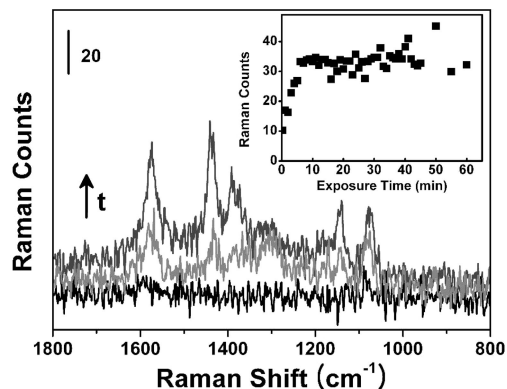


**Figure 5.** A series of Raman spectra of Ag-4ABT taken as a function of the laser exposure time using the 514.5 nm radiation as the excitation source with the laser power at the sampling position being  $\sim 0.02$  mW and the signal acquisition time being 10 s; the inset shows the growth of the 7a band of 4ABT at  $1075\text{ cm}^{-1}$  arising from Ag-4ABT taken using the 514.5 nm line of an  $\text{Ar}^+$  laser as a function of the laser exposure time.

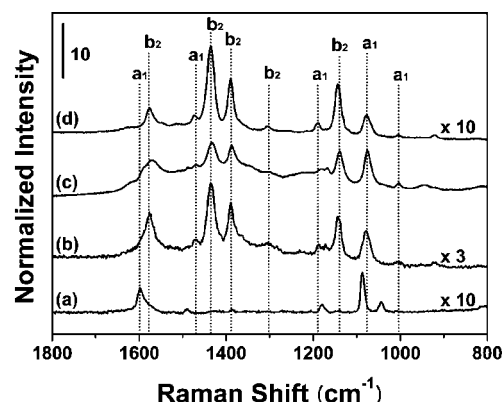


**Figure 6.** Normal Raman of Ag-4ABT taken (a) under spinning at 3000 rpm (acquisition time 10 s, laser power  $\sim 1$  mW) and SERS spectra taken in static conditions (b) using 514.5 nm radiation (acquisition time 10 s, laser power  $\sim 0.2$  mW) and (c) 632.8 nm radiation (acquisition time 10 s, laser power  $\sim 1$  mW). (d) SERS spectrum of 4ABT adsorbed on borohydride reduced Ag nanoparticles. All spectral intensities were normalized with respect to those of silicon wafers used for instrument calibration.

We also examined the possibility that the SERS-active Ag nanoaggregates produced by the irradiation of visible lasers were due to the thermolysis of Ag-4ABT salt rather than photolysis, but such a possibility appeared to be extremely low. According to the TGA and its first derivative traces as shown in Figure 7, the decomposition of Ag-4ABT proceeds at  $250^\circ\text{C}$ , suggesting that a substantial local heating is required for Ag-4ABT to be decomposed thermally by the laser light. However, the irradiation of a full-powered He/Ne laser (or  $\text{Ar}^+$  laser) on paraffin ( $\text{mp} = \sim 60^\circ\text{C}$ ) did not result in any visible degradation or melting; the maximum temperature increase monitored with thermocouples was at best  $\sim 4^\circ\text{C}$ . This observation suggests that the laser-induced local heating under our experimental conditions is not sufficient to induce the thermolysis of Ag-4ABT. Alternatively, SERS spectra of 4ABT on Ag are readily observed even when the Ag-4ABT pellets are soaked in liquid  $\text{N}_2$ , as well as in water, implying that SERS-active Ag nanoaggregates are in fact produced via photolysis rather than thermolysis.

Nonetheless, the exact mechanism by which Ag nanoaggregates are formed from silver aromatic thiolate salts ( $\text{AgS}\emptyset$ ) is a matter of conjecture. The photolysis of Ag-4ABT takes place

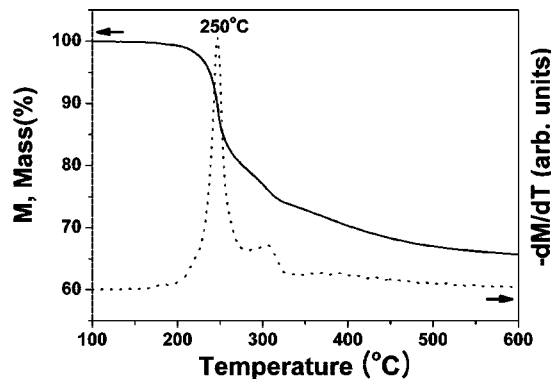


**Figure 7.** TGA (full line) and its first derivative traces (dotted line) of Ag-4ABT.

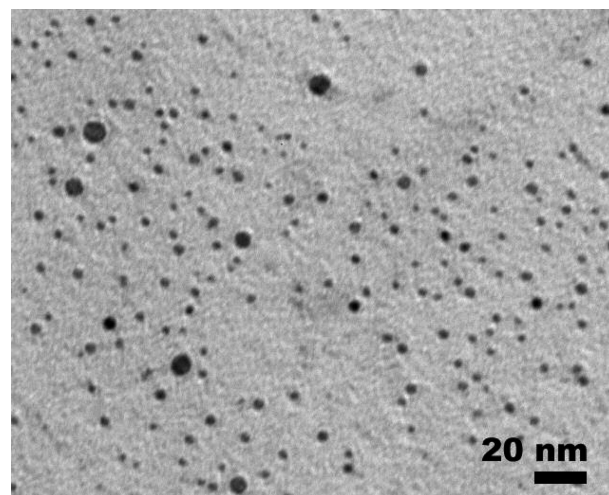
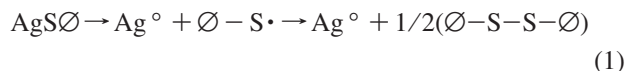


**Figure 8.** TEM image of Ag nanoparticles obtained from the photolysis of Ag-4ABT using 514.5 nm line from an  $\text{Ar}^+$  laser.

even under evacuated conditions, suggesting that the reaction has nothing to do with oxygen and water or other solvents that may be present inside the Ag-4ABT sample. The photoinduced growth of SERS-active nanoaggregates from Ag-4ABT is a complex process consisting of photoreduction of  $\text{Ag}^+$  and diffusion. The photolysis of Ag-4ABT is presumed to occur via the production of organic radicals



The Ag atoms will diffuse to one another to form Ag nanoaggregates. It is well known that organic disulfides are adsorbed very favorably onto Ag as monothiolates.<sup>30</sup> This implies that  $\emptyset - \text{S} - \text{S} - \emptyset$  formed via photolysis will immediately adsorb onto Ag nanoaggregates as monothiolates, resulting in the appearance of a SERS spectrum of an aromatic thiol ( $\emptyset\text{SH}$ ) on Ag.

To confirm the production of nanosized silver particles, a piece of pelletized Ag-4ABT that had been exposed to the 514.5 nm line of a 1 mW  $\text{Ar}^+$  laser for 10 s was immersed in a chloroform-methanol mixture, and then the mixture was shaken gently after which its decanted solution was dropped on a copper grid for the TEM measurement. As can be seen in Figure 8, nanosized silver particles are clearly observed. The sizes are polydisperse and the shapes are quite irregular. Some particles are also seen to be present in an aggregated state. These data confirm that the spectra in Figure 6b,c must be SERS spectra that have been derived from the photolysis of Ag-4ABT to give aggregated Ag nanoparticles.

When the laser intensity is low, the time dependence of the Raman intensity shows a sigmoid shape, while a semilog plot can be drawn at moderate laser intensity. Since the rate of photoproduction of neutral Ag is small with low laser intensity, a certain amount of time seems to be needed for the formation of Ag nanoaggregates which are large enough to show strong SERS effects. The rate of surface diffusion may play an important role in this case. When the laser intensity is very high, the SERS intensity grows rapidly. The rapid increase of the SERS signal in the early stage may be attributed to the synergic effect of the Ag nanoaggregates. According to the electromagnetic theory of SERS,<sup>7,8</sup> microscopic roughness on metal surfaces can increase the light intensity on the surface substantially. Enhanced field intensities at the surface can facilitate the photofragmentation of molecules adsorbed on the surface. Hence, rapid formation of Ag nanoaggregates may quicken the photoproduction of neutral Ag even further.

#### 4. Summary and Conclusion

In this investigation, we confirmed that when visible lasers are exposed to silver 4-aminobenzenethiolate (Ag-4ABT), its Raman spectrum changes over time, eventually becoming the same as the SERS spectrum of 4-aminobenzenethiol (4ABT) adsorbed on SERS-active Ag nanoparticles. The signal enhancement up to ~20 times by the exposure of lasers can be attributed to the presence of SERS-active Ag nanoparticles produced by the photoreaction of Ag-4ABT. The SERS-active Ag nanoaggregates formed by the irradiation of visible lasers were confirmed to be produced by the photolysis of Ag-4ABT salt rather than by the thermolysis. The detailed photoreaction mechanism, that the photolysis of Ag-4ABT is presumed to occur via the production of organic radicals and the reaction has nothing to do with oxygen and water or other solvents that may be present inside the Ag-4ABT sample, has also been suggested.

**Acknowledgment.** This work was supported by the Korea Science and Engineering Foundation (Grants R01-2006-000-10017-0, M10703001067-07M0300-06711, and R11-2007-012-02002-0). K.S.S. was supported by the Soongsil University Research Fund.

#### References and Notes

- (1) Haynes, C. L.; McFarland, A. D.; Van Duyne, R. P. *Anal. Chem.* **2005**, *77*, 338A.
- (2) Chang, R. K.; Furtak, T. E. *Surface Enhanced Raman Scattering*; Plenum Press: New York, 1982.
- (3) Moskovits, M. *Rev. Mod. Phys.* **1985**, *57*, 783.
- (4) Nie, S.; Emory, S. R. *Science* **1997**, *275*, 1102.
- (5) Kneipp, K.; Wang, Y.; Kneipp, H.; Perelman, L. T.; Itzkan, I.; Dasari, R. R.; Feld, M. S. *Phys. Rev. Lett.* **1997**, *78*, 1667.
- (6) Xu, H.; Bjerneld, E. J.; Käll, M.; Börjesson, L. *Phys. Rev. Lett.* **1999**, *83*, 4357.
- (7) Futamata, M.; Maruyama, Y.; Ishikawa, M. *Vib. Spectrosc.* **2002**, *30*, 17.
- (8) Jiang, J.; Bosnick, K.; Maillard, M.; Brus, L. *J. Phys. Chem. B* **2003**, *107*, 9964.
- (9) Lecomte, S.; Matejka, P.; Baron, M. H. *Langmuir* **1998**, *14*, 4373.
- (10) Campion, A.; Ivanecy, J. E.; Child, C. M.; Foster, M. J. *Am. Chem. Soc.* **1995**, *117*, 11807.
- (11) Doering, W. E.; Nie, S. *J. Phys. Chem. B* **2002**, *106*, 311.
- (12) Parikh, A. N.; Gillmor, S. D.; Beers, J. D.; Beardmore, K. M.; Cutts, R. W.; Swanson, B. I. *J. Phys. Chem. B* **1999**, *103*, 2850.
- (13) Bensebaa, F.; Ellis, T. H.; Kruus, E.; Voicu, R.; Zhou, Y. *Langmuir* **1998**, *14*, 6579.
- (14) Fijolek, H. G.; Grohal, J. R.; Sample, J. L.; Natan, M. J. *Inorg. Chem.* **1997**, *36*, 622.
- (15) Dance, I. G.; Fisher, K. J.; Banda, R. M. H.; Scudder, M. L. *Inorg. Chem.* **1991**, *30*, 183.
- (16) Baena, M. J.; Espinet, P.; Lequerica, M. C.; Levelut, A. M. *J. Am. Chem. Soc.* **1992**, *114*, 4182.
- (17) Bardeau, J. F.; Parikh, A. N.; Beers, J. D.; Swanson, B. I. *J. Phys. Chem. B* **2000**, *104*, 627.
- (18) Bensebaa, F.; Ellis, T. H.; Kruus, E.; Voicu, R.; Zhou, Y. *Can. J. Chem.* **1998**, *76*, 1654.
- (19) Lee, S. J.; Han, S. W.; Choi, H. J.; Kim, K. *Eur. Phys. J. D* **2001**, *16*, 293.
- (20) Lee, S. J.; Han, S. W.; Choi, H. J.; Kim, K. *J. Phys. Chem. B* **2002**, *106*, 2892.
- (21) Seo, Y. U.; Lee, S. J.; Kim, K. *J. Phys. Chem. B* **2004**, *108*, 4000.
- (22) Joo, T. H.; Kim, M. S.; Kim, K. *J. Raman Spectrosc.* **1987**, *18*, 57.
- (23) Lee, T. G.; Yeom, H. W.; Oh, S.-J.; Kim, K.; Kim, M. S. *Chem. Phys. Lett.* **1989**, *163*, 98.
- (24) Park, H.; Lee, S. B.; Kim, K.; Kim, M. S. *J. Phys. Chem.* **1990**, *94*, 7576.
- (25) Lee, P. C.; Meisel, D. *J. Phys. Chem.* **1982**, *86*, 3391.
- (26) Osawa, M.; Matsuda, N.; Yoshii, K.; Uchida, I. *J. Phys. Chem.* **1994**, *98*, 12702.
- (27) Zhou, Q.; Zhao, G.; Chao, Y.; Li, Y.; Wu, Y.; Zheng, J. *J. Phys. Chem. C* **2007**, *111*, 1951.
- (28) Creighton, J. A. *Surf. Sci.* **1983**, *124*, 209.
- (29) Moskovits, M.; Suh, J. S. *J. Phys. Chem.* **1984**, *88*, 5526.
- (30) Joo, T. H.; Kim, K.; Kim, M. S. *J. Mol. Struct.* **1987**, *162*, 191.
- (31) Varsanyi, G. *Vibrational Spectra of Benzene Derivatives*; Academic Press: New York, 1969.

JP802712R